

q -breathers in discrete nonlinear Schrödinger lattices

K G Mishagin¹, S Flach², O I Kanakov¹ and M V Ivanchenko^{1,3}

¹ Department of Radiophysics, Nizhny Novgorod University, Gagarin Avenue, 23, 603950 Nizhny Novgorod, Russia

² Max Planck Institute for the Physics of Complex Systems, Nöthnitzer Strasse 38, D-01187 Dresden, Germany

³ Department of Applied Mathematics, University of Leeds, Leeds LS2 9JT, UK
E-mail: flach@pks.mpg.de

New Journal of Physics **10** (2008) 073034 (21pp)

Received 19 March 2008

Published 18 July 2008

Online at <http://www.njp.org/>

doi:10.1088/1367-2630/10/7/073034

Abstract. q -breathers (QBs) are exact time-periodic solutions of extended nonlinear systems continued from the normal modes of the corresponding linearized system. They are localized in the space of normal modes. The existence of these solutions in a weakly anharmonic atomic chain explained essential features of the Fermi–Pasta–Ulam (FPU) paradox. We study QBs in one-, two- and three-dimensional discrete nonlinear Schrödinger (DNLS) lattices—theoretical playgrounds for light propagation in nonlinear optical waveguide networks, and the dynamics of cold atoms in optical lattices. We prove the existence of these solutions for weak nonlinearity. We find that the localization of QBs is controlled by a single parameter which depends on the norm density, nonlinearity strength and seed wave vector. At a critical value of that parameter QBs delocalize via resonances, signaling a breakdown of the normal mode picture and a transition into the strong mode–mode interaction regime. In particular, this breakdown takes place at one of the edges of the normal mode spectrum, and in a singular way also in the center of that spectrum. A stability analysis of QBs supplements these findings. We relate our findings to previous studies of time-periodic multibreather standing waves. For three-dimensional lattices, we find QB vortices which violate time reversal symmetry and generate a vortex ring flow of energy in normal mode space.

Contents

1. Introduction	2
1.1. Background	2
1.2. Motivation	3
1.3. Aim	3
2. Model	4
3. Proof of existence of t-reversible QB solutions for weak nonlinearity	5
4. Perturbation theory for QB profiles	6
4.1. Close to the band edges	6
4.2. Close to the band center	8
5. QBs for $d = 1$: results	9
5.1. Close to the band edge	9
5.2. Close to the center of the band	12
5.3. Stability of QBs	13
6. Periodic boundary conditions	14
7. QBs in two- and three-dimensional lattices	15
8. QBs and time-periodic multibreather standing waves	17
9. Discussion	18
9.1. Scales, delocalization thresholds and healing length of a BEC	18
9.2. Delocalization thresholds and modulational instability	19
9.3. Comparing analytical and numerical results	19
9.4. Open questions	20
Acknowledgments	20
References	20

1. Introduction*1.1. Background*

In 1955, Fermi, Pasta and Ulam (FPU) published their seminal report on the absence of thermalization in arrays of particles connected by weakly nonlinear springs [1]. In particular they observed that energy, initially seeded in a low-frequency normal mode of the linear problem with a frequency ω_q and corresponding normal mode number q , stayed almost completely locked in a few neighbor modes in frequency space, instead of being distributed quickly among all modes of the system. The latter expectation was due to the fact that nonlinearity induces a long-range network of interactions among the normal modes. From the present perspective, the FPU problem appears to consist of the following parts: (i) for certain parameter ranges (energy, system size, nonlinearity strength and seed mode number), excitations appear to stay *exponentially localized* in q -space of the normal modes for *long but finite* times [2]; (ii) this *intermediate* localized state is reached on a fast timescale τ_1 , and *equipartition is reached* on a second timescale τ_2 , which can be many orders of magnitude larger than τ_1 [3]; (iii) tuning the control parameters may lead to a drastic shortening of τ_2 , until both timescales merge, and the metastable regime of localization is replaced by a fast relaxation towards thermal

equilibrium [3], which is related to the nonlinear resonance overlap estimated by Izrailev and Chirikov [4]. FPU happened to compute cases with values of τ_2 which were inaccessible within their computation time. Among many other intriguing details of the evolution of the intermediate localized state, we mention the possibility of having an almost regular dynamics of the few strongly excited modes, leading to the familiar phenomenon of beating. This beating manifests as a recurrence of almost all energy into the originally excited mode (similar to the beating among two weakly coupled harmonic oscillators), and was explained by Zabusky and Kruskal with the help of real space solitons of the Korteweg–de-Vries (KdV) equation, for a particular case of long wavelength seed modes, and periodic boundary conditions [5]. The regular dynamics may be replaced by a weak chaotic one upon crossing yet another threshold in control parameters [6]. Remarkably, the weak chaos is still confined to the core of the localized excitation, leaving the exponential localization almost unchanged, and perhaps influencing most strongly the parameter dependence of τ_2 . The interested reader may also refer to [7].

1.2. Motivation

Single-site excitations in translationally invariant lattices of interacting anharmonic oscillators are known to show a similar behavior of trapping the excitation on a few lattice sites around the originally excited one [8]. As conjectured almost 40 years ago [9], exact time-periodic and spatially localized orbits—*discrete breathers* (also *intrinsic localized modes* and *discrete solitons*) persist in such lattices, and the dynamics on such an orbit, as well as the dynamics of the nearby phase space flow, account for many observations, and have found application in many different areas of physics [10]. Recently, it was shown that the regime of localization in normal mode space for the FPU problem can be equally explained by obtaining *q-breathers* (QBs)—time-periodic and modal-space-localized orbits—which persist in the FPU model for nonzero nonlinearity [11]. The originally computed FPU trajectory stays close to such QB solutions for a long time, and therefore many features of its short- and medium-time dynamics have been shown to be captured by the QB solution and small phase-space fluctuations around it. Delocalization thresholds for QBs are related to resonances, and corresponding overlap criteria [11]. The method of constructing QB solutions was generalized to two- and three-dimensional FPU lattices [12]. Most importantly, a scaling theory was developed, which allowed to construct QBs for arbitrarily large system sizes, and to obtain analytical estimates on the degree of localization of these solutions for macroscopic system size [13]. Expectations were formulated, that the existence of QBs should be generic to many nonlinear spatially extended systems.

1.3. Aim

The spectrum of normal mode frequencies of the linear part of the FPU model is acoustic and contains zero, reflecting the fact that the model conserves total mechanical momentum. In addition it is bounded by a lattice-induced cut-off, the analogue of the Debye cutoff in solid state physics. We may think of two pathways of extending the above discussed results to other system classes. First, we could consider a spatially continuous system, instead of a lattice. However, the initial FPU studies showed confinement to a few long wavelength modes, and the results of Zabusky and Kruskal [5], confirm that indeed in the spatially continuous system (KdV), trajectories similar to the FPU trajectory persist.

As discussed above, the persistence, localization, and delocalization of QBs is due to a proper avoiding of, or harvesting on, resonances between normal modes. It therefore appears to be of substantial interest to extend the previous results to systems with a qualitatively different normal mode spectrum. Such a spectrum is the one which does not contain zero, and is called optical. It may correspond to the excitation of certain degrees of freedom in a complex system, or to an FPU type model which is deposited on some substrate, or otherwise exposed to some external fields. Together with the acoustic band, these two band structures, when combined, describe almost any type of normal mode spectrum in a linear system with spatially periodic modulated characteristics.

Adding weak nonlinearities to such a system, taking local action angle representations, and performing various types of multiple scale analysis, such models are mapped on discrete nonlinear Schrödinger (DNLS) models [14, 15]. These models enjoy a gauge invariance, and a conservation of the sum of the local actions (norms), i.e. some global norm. A particular version of these equations is known as the discrete Gross–Pitaevsky equation, and is derived on mean field grounds for Bose–Einstein condensates (BEC) of ultracold bosonic atoms in optical lattices [16, 17]. The norm is simply the conserved number of atoms in this case, and the nonlinearity derives from the atom–atom interaction. The propagation of light in (spatially modulated) optical media is another research area where DNLS models are used [18]. In that case the norm conservation derives from the conservation of electromagnetic wave energy along the propagation distance (in the assumed absence of dissipative mechanisms). But DNLS models served equally well in many other areas of physics, where weak interactions start to play a role, e.g. in the theory of polaron formation due to electron–phonon interaction in solids.

Morgante *et al* and Johansson *et al* studied time-periodic multibreather standing waves [15]. These solutions are encoded by a pattern in real space for infinitely large lattices. They are continued from the limit of zero intersite coupling. We will relate these solutions to the QB solutions, which are encoded by a single normal mode number at the limit of zero nonlinearity.

Releasing the norm conservation (e.g. by allowing the number of atoms in a condensate to fluctuate) will reduce the symmetries of the corresponding model, but most importantly, it will lead to possible new resonances of higher harmonics. We will discuss these limitations, and possible effects of releasing these limitations on QBs, in the discussion section.

A particular consequence of norm conservation is a corresponding symmetry of the normal mode spectrum, which relates both (upper and lower) band edges, and makes the band center a symmetry point as well.

The paper is structured as follows: section 2 introduces the model and the main equations of motion. Section 3 gives an existence proof for QBs. In section 4, we derive analytical expressions for the QB profiles using perturbation theory. These are compared with the numerical results for $d = 1$ in section 5, which also contains a stability analysis of the obtained periodic orbits. Section 6 gives results on periodic boundary conditions (as opposed to fixed boundaries). We generalize to $d = 2, 3$ in section 7. In section 8, we relate QB solutions to results on time-periodic multibreather standing waves, and discuss all results in section 9.

2. Model

We consider a DNLS equation on a d -dimensional hypercubic lattice of linear size N :

$$i\dot{\psi}_n = \sum_{m \in D(n)} \psi_m + \mu |\psi_n|^2 \psi_n. \quad (1)$$

Here, ψ is a complex scalar which may describe e.g. the probability amplitude of an atomic cloud on an optical lattice site [17], or relates to the amplitudes of a propagating electromagnetic wave in an optical waveguide [18]. The lattice vectors \mathbf{n} , \mathbf{m} have integer components, and $D(\mathbf{n})$ is the set of nearest neighbors for the lattice site \mathbf{n} . If not noted otherwise, we consider fixed boundary conditions: $\psi_{\mathbf{n}} = 0$, if $n_l = 0$ or $n_l = N + 1$ for any of the components of \mathbf{n} . Equation (1) is derived from the Hamiltonian

$$H = \sum_{\mathbf{n}} \left(\sum_{\mathbf{m} \in D(\mathbf{n})} \psi_{\mathbf{m}} \psi_{\mathbf{n}}^* + \frac{\mu}{2} |\psi_{\mathbf{n}}|^4 \right), \quad (2)$$

using the equations of motion $i\dot{\psi}_{\mathbf{n}} = \partial H / \partial \psi_{\mathbf{n}}^*$. In addition to energy, equation (1) conserves the norm $B = \sum_{\mathbf{n}} |\psi_{\mathbf{n}}|^2$. Note that the change of the nonlinearity parameter μ in (1) is strictly equivalent to changing the norm B . Here, we will keep the norm B (alternatively the norm density) fixed, and vary μ .

We perform a canonical transformation to the reciprocal space of normal modes (q -space of size N^d) with new variables $Q_{\mathbf{q}}(t) \equiv Q_{q_1 \dots q_d}(t)$

$$\psi_{\mathbf{n}}(t) = \left(\frac{2}{N+1} \right)^{d/2} \sum_{q_1, \dots, q_d=1}^N Q_{\mathbf{q}}(t) \prod_{i=1}^d \sin \left(\frac{\pi q_i n_i}{N+1} \right). \quad (3)$$

Together with (1) we obtain the following equations of motion in normal mode space:

$$i\dot{Q}_{\mathbf{q}} = -\omega_{\mathbf{q}} Q_{\mathbf{q}} + \frac{2^{d-2}\mu}{(N+1)^d} \sum_{\mathbf{p}, \mathbf{r}, \mathbf{s}} C_{\mathbf{q}, \mathbf{p}, \mathbf{r}, \mathbf{s}} Q_{\mathbf{p}} Q_{\mathbf{r}}^* Q_{\mathbf{s}}, \quad (4)$$

where $\omega_{\mathbf{q}} = -2 \sum_{i=1}^d \cos \frac{\pi q_i}{N+1}$ are the normal mode frequencies for the linearized system (1) with $\mu = 0$. Nonlinearity introduces a network of interactions among the normal mode oscillators with the following coupling coefficients:

$$C_{\mathbf{q}, \mathbf{p}, \mathbf{r}, \mathbf{s}} = \prod_{i=1}^d C_{q_i, p_i, r_i, s_i},$$

$$C_{q_i, p_i, r_i, s_i} = \sum_{k, l, m=0}^1 (-1)^{k+l+m} \left(\delta_{(-1)^k p_i + (-1)^l r_i + (-1)^m s_i, q_i} + \delta_{(-1)^k p_i + (-1)^l r_i + (-1)^m s_i, q_i \pm (2N+2)} \right). \quad (5)$$

3. Proof of existence of t -reversible QB solutions for weak nonlinearity

We look for exact time-periodic solutions, which are stationary solutions of the DNLS equation (1), and which are localized in normal mode space: $\psi_{\mathbf{n}}(t) = \phi_{\mathbf{n}} \exp(i\Omega t)$ with frequency Ω and time-independent amplitudes $\phi_{\mathbf{n}}$. In the space of normal modes these stationary solutions have the form $Q_{\mathbf{q}}(t) = A_{\mathbf{q}} \exp(i\Omega t)$, where the amplitudes of modes $A_{\mathbf{q}}$ are time-independent and related to the real-space amplitudes by the transformation (3). At a given norm B they satisfy a system of algebraic equations:

$$\begin{cases} -\Omega A_{\mathbf{q}} + \omega_{\mathbf{q}} A_{\mathbf{q}} - \frac{2^{d-2}\mu}{(N+1)^d} \sum_{\mathbf{p}, \mathbf{r}, \mathbf{s}} C_{\mathbf{q}, \mathbf{p}, \mathbf{r}, \mathbf{s}} A_{\mathbf{p}} A_{\mathbf{r}}^* A_{\mathbf{s}} = 0, & q_1, \dots, q_d = \overline{1, N}, \\ \sum_{\mathbf{q}} |A_{\mathbf{q}}|^2 - B = 0. \end{cases} \quad (6)$$

We are focusing here (and throughout almost all of the paper) on t -reversible periodic orbits. Therefore, we may consider all A_q to be real numbers. In this case, system (6) contains $N + 1$ equations for $N + 1$ variables. This system can be condensed into an equation for a vector function:

$$\mathbf{F}(\mathbf{X}; \mu, B) = 0 \quad (7)$$

with $\mathbf{X} = \{\dots, A_q, \dots, \Omega\}$. The components of \mathbf{F} are the left-hand sides of (6), while μ, B are parameters.

For $\mu = 0$ the normal modes in (4) are decoupled and each oscillator conserves its norm in time: $B_q(t) = A_q^2$. Let us consider the excitation of only one of the oscillators with the seed mode number \mathbf{q}_0 : $B_q = B_{\mathbf{q}_0} \delta_{q, \mathbf{q}_0}$. The excited normal mode is a time-periodic solution of (4), and is localized in \mathbf{q} -space. According to the implicit function theorem [19], the corresponding solution of (6) can be continued into the nonlinear case ($\mu \neq 0$), if the Jacoby matrix of the linear solution $(\partial \mathbf{F} / \partial \mathbf{X})_{\mu=0, B}$ is invertible, i.e. $\|\partial \mathbf{F} / \partial \mathbf{X}\|_{\mu=0, B} \neq 0$. The Jacobian

$$\left\| \frac{\partial \mathbf{F}}{\partial \mathbf{X}} \right\|_{\mu=0} = (-1)^{N^d+1} 2A_{\mathbf{q}_0}^2 \prod_{q \neq \mathbf{q}_0} (\omega_q - \omega_{\mathbf{q}_0}). \quad (8)$$

Therefore, the continuation of a linear mode with the seed mode number \mathbf{q}_0 will be possible if $\omega_q \neq \omega_{\mathbf{q}_0}$, for all $\mathbf{q} \neq \mathbf{q}_0$. That condition holds for the case $d = 1$, and thus QBs exist at least for suitably small values of μ there. For higher dimensions, degeneracies of normal mode frequencies appear. These degeneracies are not an obstacle for numerical continuation of QBs, but a formal persistence proof has to deal with them accordingly. Analogous results for two- and three-dimensional β -FPU lattices have been obtained in [12].

4. Perturbation theory for QB profiles

To analyze the localization properties of QBs in \mathbf{q} -space we use a perturbation theory approach similar to [11, 12]. We consider the general case of a d -dimensional DNLS lattice (1). Taking the solution for a linear normal mode with number $\mathbf{q}_0 = (q_{1,0}, \dots, q_{d,0})$ as a zero-order approximation, an asymptotic expansion of the solution to the first N equations of (6) in powers of the small parameter $\sigma = \mu 2^{(d-2)} / (N+1)^d$ is implemented. Note that in the same way as it was done in [11, 12], we fix the amplitude of the seed mode $A_{\mathbf{q}_0}$. Later on we will apply the norm conservation law (the last equation of (6)) to express the norm $B_{\mathbf{q}_0} = |A_{\mathbf{q}_0}|^2$ via the total norm B for the case of $d = 1$. Analytical estimations presented below describe amplitudes of modes located along the directions of the lattice axes starting from the mode \mathbf{q}_0 . Mode amplitudes of QBs have the slowest decay along these directions (see section 7). Studying QB localization along a chosen dimension i , for the sake of compactness we will use a scalar mode number to denote the i th component of \mathbf{q} , assuming all other components be the same as in \mathbf{q}_0 : $q_{j \neq i} = q_{j,0}$.

4.1. Close to the band edges

Let us start with QBs localized in the low-frequency mode domain ($q_{i,0} \ll N$, $i = \overline{1, d}$). According to the selection rules, if the seed mode number $q_{i,0}$ is even (odd), then only even (odd) modes are excited along i th dimension. The n th order of the asymptotic expansion is the leading one for the mode $q_{i,n} = (2n+1)q_{i,0}$. When q_i reaches the upper band edge in the

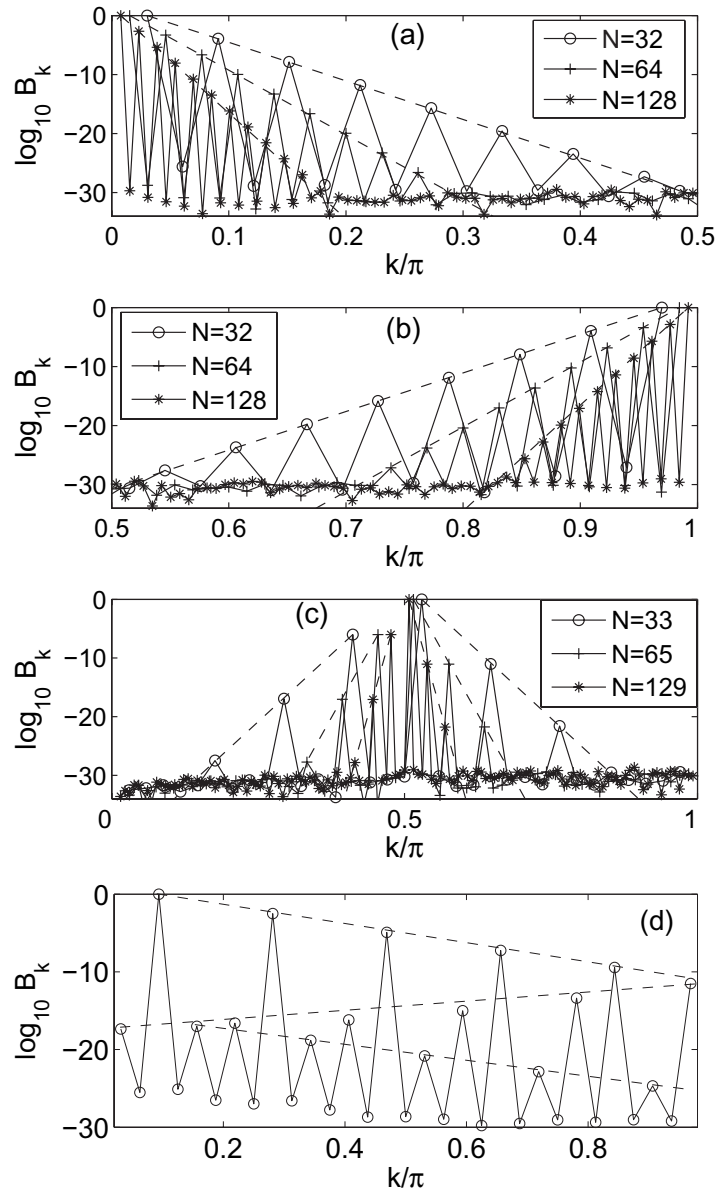


Figure 1. Distributions of mode norms for QBs in the one-dimensional DNLS model with parameters: $B = 1$, $\mu = 0.1$ for (a)–(c); (a) QBs with low-frequency seed mode $q_0 = 1$, (b) QBs with high-frequency seed mode $q_0 = N$ and (c) QBs with seed mode near the middle of the spectrum $q_0 = 1 + (N+1)/2$. Dashed lines in (a)–(c) correspond to analytical estimations. (d) Observation of multiple reflections at the boundaries of the q -space, $N = 31$, $B = 1$, $\mu = 2$ and $q_0 = 3$. Dashed lines in (d) are guidelines for the eye.

i th-direction, a reflection at the edge in q -space takes place if $N+1$ is not divisible by $q_{i,0}$ (cf figure 1(d)). If $N+1$ is divisible by $q_{i,0}$ then only modes $q_{i,n} = (2n+1)q_{i,0} < N$ are excited. In the analytical estimates, we assume a large enough lattice size. Then the effect of band edge reflections is appearing in higher orders of the perturbation, which will not be considered.

In this case the approximate solution is

$$A_{(2n+1)q_{i,0}} = (-\text{sign}(\mu))^n \left(\sqrt{\lambda_d^{(i)}} \right)^n A_{q_0}, \quad i = \overline{1, d}, \quad \Omega = \omega_{q_0} - \sigma A_{q_0}^2 + O(\sigma^2). \quad (9)$$

The corresponding exponential decay of mode norms is

$$B_{(2n+1)q_{i,0}} = \left(\lambda_d^{(i)} \right)^n B_{q_0}, \quad \sqrt{(\lambda_d^{(i)})} = \frac{|\mu| A_{q_0}^2 (N+1)^{2-d}}{2^{5-d} \pi^2 (q_{i,0})^2} = \frac{|\mu| b_{k_0}}{2^{5-d} (k_{i,0})^2}, \quad i = \overline{1, d}. \quad (10)$$

$\lambda_d^{(i)}$ ($0 < \lambda_d^{(i)} < 1$) characterize the exponential decay along the i th dimension. Here, $k_{i,0} = \frac{\pi q_{i,0} (2n+1)}{N+1}$ is the i th component of the seed wave vector \mathbf{k}_0 , and $b_{k_0} = B_{k_0} / (N+1)^d$ is the norm density of the seed mode. When using intensive quantities—wave number $k_{i,0}$ and norm density b_{k_0} —only, λ does not depend on the system size.

Equation (4) is invariant under the symmetry operation $\mu \rightarrow -\mu$, $t \rightarrow -t$ and $q_{i,0} \rightarrow N+1 - q_{i,0}$ for all $i = \overline{1, d}$, which changes the sign of nonlinearity, and maps modes from one band edge to the other. The replacement $q_{i,0} \rightarrow N+1 - q_{i,0}$ for all $i = \overline{1, d}$ in (6) is equivalent to substitutions $\mu \rightarrow -\mu$ and $\Omega \rightarrow -\Omega$. Using this symmetry, we can easily apply the above results to the case of QBs localized near the upper band edge, by counting mode indices from the upper edge: $\tilde{q}_i = N+1 - q_i$. We neglect reflections from the lower band edge, such that only modes with numbers $\tilde{q}_{i,n} = (2n+1)\tilde{q}_{i,0}$ (n is integer, $\tilde{q}_{i,0} \ll N$) are assumed to be excited. It follows:

$$A_{N+1-\tilde{q}_{i,n}} = (\text{sign}(\mu))^n \left(\sqrt{\tilde{\lambda}_d^{(i)}} \right)^n A_{q_0}, \quad (11)$$

where n is an integer and

$$\sqrt{(\tilde{\lambda}_d^{(i)})} = \frac{|\mu| A_{q_0}^2 (N+1)^{2-d}}{2^{5-d} \pi^2 (N+1 - q_{i,0})^2} = \frac{|\mu| b_{k_0}}{2^{5-d} (\pi - k_{i,0})^2}, \quad i = \overline{1, d}. \quad (12)$$

The analytical expression for the frequency of the QB solution turns out to be the same as for the case of small seed mode numbers.

4.2. Close to the band center

We implement the perturbation theory approach for seed modes close to the band center. Let us first consider the case of odd N . We introduce the new index p^i , which is the number of a mode counted from the middle of the spectrum along the i th dimension: $p_i = q_i - (N+1)/2$. We choose the seed mode with $|p_{i,0}| \ll (N+1)/2$. In the n th order of perturbation theory the newly excited mode along the i th dimension has the number $p_{i,n} = (-1)^n (2n+1) p_{i,0}$, and

$$A_{p_{i,2n}} = (-\lambda_d^{(i)})^n A_{p_{i,0}}, \quad A_{p_{i,2n+1}} = \text{sign}(p_{i,0}) (-1)^{n+1} (\lambda_d^{(i)})^{n+1/2} A_{p_{i,0}}, \quad (13)$$

where $i = \overline{1, d}$, $\lambda_d^{(i)} > 0$, $n = 1, 2, 3, \dots$, and

$$\sqrt{\lambda_d^{(i)}} = \frac{|\mu| A_{q_0}^2}{2^{4-d} \pi |q_{i,0} - (N+1)/2|} = \frac{|\mu| b_{k_0}}{2^{4-d} |k_{i,0} - \pi/2|}. \quad (14)$$

When using intensive quantities, λ again does not depend on the system size.

For the case of even N , we use $p_i = q_i - N/2$ and assume that the seed mode index $p_{i,0} > 0$, $i = \overline{1, d}$. The set of consecutively perturbed modes becomes

$$p_{i,0} \rightarrow (-3p_{i,0} + 2) \rightarrow (5p_{i,0} - 2) \rightarrow (-7p_{i,0} + 4) \rightarrow (9p_{i,0} - 4) \rightarrow (-11p_{i,0} + 6) \rightarrow \dots \quad (15)$$

In the n th order of perturbation theory the number of the new excited mode along the i th dimension $p_{i,n}$ satisfies $P_{i,n} - \frac{1}{2} = (-1)^n(2n+1)(p_{i,0} - \frac{1}{2})$, $n = 1, 2, \dots$. The amplitudes satisfy (13), but with

$$\sqrt{\lambda_d^{(i)}} = \frac{|\mu|A_{q_0}^2}{2^{4-d}\pi|q_{i,0} - N/2|} = \frac{|\mu|b_{k_0}}{2^{4-d}|k_{i,0} - \pi/2 + \pi/(2N+2)|}. \quad (16)$$

For large enough N equation (16) approaches the expression (14), therefore we will use (14) for large N only.

5. QBs for $d = 1$: results

5.1. Close to the band edge

The key property of QBs is that they are localized in the space of linear normal modes. Note that some QB solutions may be compact in q -space and contain only one seed mode q_0 ,⁴ or a few modes additionally, due to symmetries of the interaction network spanned by the nonlinear terms [20].

Let us consider the one-dimensional case. We compute QBs as the solutions of the nonlinear equations (6) using the single-mode solution for $\mu = 0$ as an initial approximation. figures 1(a) and (b) show the distribution of mode norms for QBs in the space of wave numbers $k = \pi q/(N+1)$ for different chain sizes and different seed wave numbers, located near the lower ($k_0 \ll \pi$, figure 1(a)) and upper ($\pi - k_0 \ll \pi$, figure 1(b)) edges of the linear mode spectrum.

We find exponential localization of QBs, with a localization length which depends strongly on the chosen parameters. The obtained analytical estimations for QBs localized at the lower band edge (9) and (10), respectively, upper band edge (11) and (12), are in quantitative agreement with numerical results (see dashed lines in figures 1(a) and (b)).

The exponential decay in (10) depends on the seed mode norm density. Many applications (e.g. cold atoms in a condensate) rather fix the total norm, or total norm density. For the obtained QB solutions with $q_0 \ll N$, the relation between these quantities can be estimated by the sum of infinite geometric series:

$$B \approx \sum_{n=0}^{\infty} \lambda^n B_{q_0} = \frac{B_{q_0}}{1-\lambda}, \quad (17)$$

where $\lambda \equiv \lambda_1^{(1)}$. From (17) it follows that $b_{k_0} = (1-\lambda)b$, where $b = B/(N+1)$ is the total norm density. Substituting the expression for b_{k_0} into (10) and solving the equation for $\sqrt{\lambda}$ we obtain:

$$\sqrt{\lambda} = \frac{\sqrt{1+4v^4/k_0^4} - 1}{2v^2/k_0^2}, \quad v^2 = \frac{|\mu|b}{16}. \quad (18)$$

The same dependence of $\sqrt{\lambda}$ on k_0 was obtained for low-frequency QBs in the β -FPU model [13]. The exponential decay of mode norms in the space of wave numbers, can be now

⁴ QBs with seed linear modes $q_{0i} = (N+1)/3, (N+1)/2, 2(N+1)/3$ ($|i = \overline{1, d}|$) are compact in q -space because these seed modes do not excite the other modes due to the selection rules (5).

written for QBs localized in low-frequency modes:

$$\ln b_k = \left(\frac{k}{k_0} - 1 \right) \ln \sqrt{\lambda} + \ln b_{k_0}. \quad (19)$$

To characterize the degree of localization in k -space, we use the slope of the profile of mode norms in log-normal plots (19) – S [13], where the absolute value of S is equivalent to the inverse value of the localization length ξ :

$$S = \frac{1}{k_0} \ln \sqrt{\lambda}, \quad |S| \equiv \xi^{-1}. \quad (20)$$

Substituting the expression for $\sqrt{\lambda}$ (18) into (20) we obtain:

$$S = \frac{1}{\nu z} \ln \left(\sqrt{1 + z^4/4} - z^2/2 \right), \quad z = k_0/\nu. \quad (21)$$

Therefore, the slope (inverse localization length) is a function of the rescaled wave number z . It therefore parametrically depends on just one effective nonlinearity parameter ν , which is given by the product of the total norm density and the absolute value of nonlinearity strength. S vanishes for $z \rightarrow 0$, and it has an extremum $\min(S) \approx -0.7432/\nu$ at $z_{\min} \approx 2.577$. The wave number $k_0 = k_{\min} \equiv z_{\min} \nu$ corresponds to the strongest localization of a QB with fixed effective nonlinear parameter ν . With increasing ν the localization length increases. Most importantly, the localization length diverges for small $k_0 \ll k_{\min}$ since $|S| \approx z/(2\nu)$ in that case. This delocalization is due to resonances with nearby normal modes close to the band edge. Note that our analytical estimations do not depend on the sign of the nonlinearity parameter μ .

In figures 1(a) and (b), due to the small sizes of the chain, all values of k_0 are greater than k_{\min} , so a monotonous dependence of the slope on k_0 is observed. In figure 2, we plot theoretical and numerically obtained dependencies $S(k_0)$ for different values of the nonlinear parameter μ and different system sizes N (we use large enough N to resolve the theoretically predicted extremum of S). In all cases the numerical results show that the slopes indeed are characterized by intensive quantities only, and the above derived scaling laws hold.

For positive values of μ and seed wave numbers close to the lower band edge, the extremum in S is reproduced in the numerical data, though the numerical curves deviate from theoretical curves for small k_0 . We also find that k_{\min} increases and $|S(k_{\min})|$ decreases with increasing μ as predicted by our analytical results (increase of norm density b gives the same effect).

For negative values of μ and seed wave numbers close to the lower band edge, we do not observe an extremum for S . In the region of small k_0 the numerically obtained curves for positive and negative values of μ differ, while the theoretically predicted slopes do not depend on the sign of μ . Figure 3 shows the mode norm profiles of QB solutions with small k_0 obtained for positive and negative values of μ . The reason for the discrepancy between theoretical prediction and numerical results for negative values of μ must be strong contributions from higher order terms in the perturbation expansion. The standard argument is that the perturbation theory is valid if the localization length is small, i.e. $|\lambda| \ll 1$ as well. When $|\lambda|$ becomes of the order of one, higher order terms in perturbation theory have to be taken into account, and it would be tempting to conclude that delocalization will take place. That should be true especially when all higher order terms in the series carry the same sign. That is the case for positive nonlinearity here, but for negative μ we obtain alternating signs of higher order terms. These alternating signs therefore effectively cancel most of the terms in the series, and are responsible for an increasing localization of QBs with negative μ in the limit of small wave numbers.

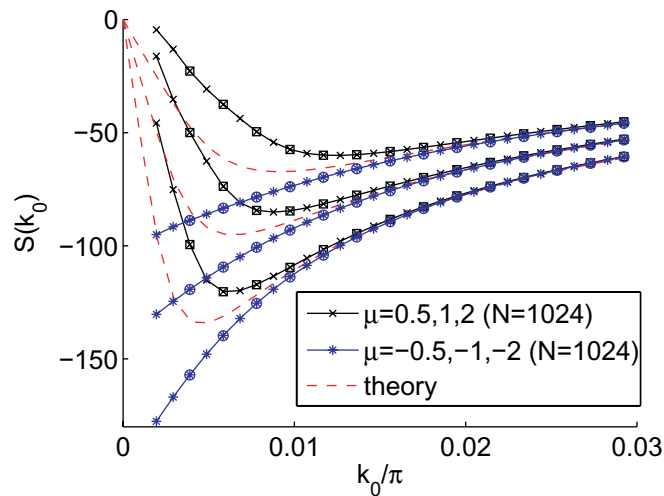


Figure 2. The slope S as a function of the seed wave number k_0 for $d = 1$ with fixed norm density $b = 1/1025$, $\mu = \pm 0.5, \pm 1$ and ± 2 (from bottom to top). Dashed lines correspond to the analytical estimates. Different symbols: slope from the numerical calculation of QB (squares and circles represent the results for $N = 512$). Solid lines guide the eye.

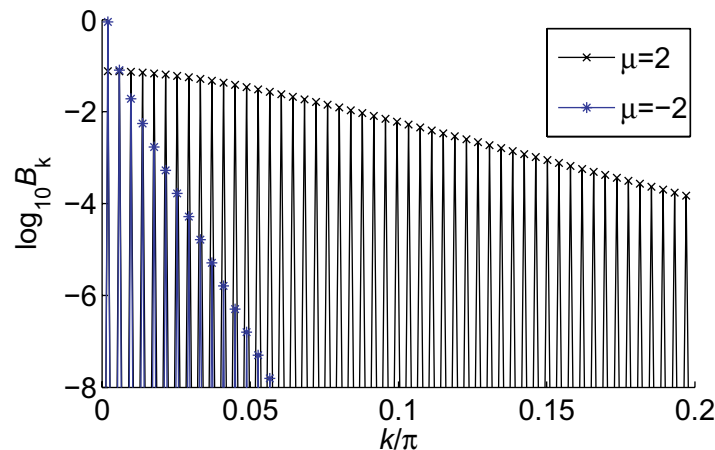


Figure 3. Distributions of mode norms for QBs in the one-dimensional DNLS model for positive and negative values of μ ; $q_0 = 2$, $b = 1/1025$ and $N = 1024$.

The obtained results for QBs with seed wave numbers close to the lower band edge ($k_0 \ll \pi$) are valid for the case of k_0 close to the upper band edge ($\pi - k_0 \ll \pi$) if we change $\mu \rightarrow -\mu$. Thus, there is a strong asymmetry in the localization properties of QB solutions with $k_0 < \pi/2$ and $k_0 > \pi/2$ for a fixed sign of nonlinearity.

The numerical results in figure 2 show that slope values calculated for different system sizes lie on the same curves with corresponding μ even in the region of small k_0 , where higher order corrections to our analytical estimates have to be taken into account. This result is in agreement with the exact scaling of QB solutions described in [13]. We plot in figure 4 the master slope function $S_m(z) = \nu S$, which depends on a single variable z [13]. It implies that

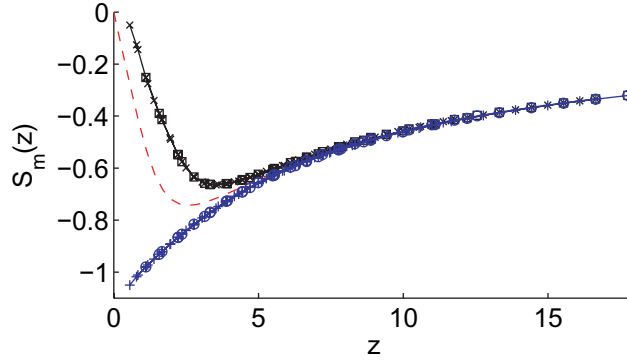


Figure 4. The master slope function $S_m(z)$ (dashed line). Different symbols and eye-guiding solid lines correspond to the scaled numerical estimates of the slope presented in figure 2 (bottom line, $\mu < 0$; top line, $\mu > 0$).

knowing this single master slope function is sufficient to predict the localization property of a QB at any seed wave number $k_0 \ll \pi$, at any energy etc. Numerically obtained slopes presented in figure 2 are rescaled and plotted in figure 4. We see that all results corresponding to the same sign of μ condense on a single curve even (and especially) for small k_0 , though these numerical results differ from the analytical estimation.

5.2. Close to the center of the band

Figure 1(c) shows the distribution of mode norms for QBs in the space of wave numbers $k = \pi q/(N+1)$ for different chain sizes and different seed wave numbers, located close to the center of the spectrum ($|k_0 - \pi/2| \ll \pi$). The analytical estimation for the amplitudes of these QBs are in good quantitative agreement with the numerical results, for small enough parameters μ and b , cf figure 1(c).

We express again the norm density of the seed mode via the total norm density: $b_{k_0} = (1 - \lambda)b$, ($\lambda \equiv \lambda_1^{(1)}$). Substituting this expression into (14) we find:

$$\sqrt{\lambda} = \frac{\sqrt{1 + 4\nu^2/(k_0 - \pi/2)^2} - 1}{2\nu/|k_0 - \pi/2|}, \quad \nu = \frac{|\mu|b}{8}. \quad (22)$$

The slope of the mode norm profile in k -space is given by

$$S = \frac{1}{|k_0 - \pi/2|} \ln \sqrt{\lambda} = \frac{1}{2\nu z} \ln \left(\sqrt{1 + z^2} - z \right), \quad (23)$$

where $z = |k_0 - \pi/2|/(2\nu)$. For $z \ll 1$: $S = (-1 + z^2/6 + O(z^4))/(2\nu)$, for $z \gg 1$: $S = \ln(1/(2z) + O(1/z^3))/(2\nu z)$. In the limit $z \rightarrow 0$, the slope $S \rightarrow -1/(2\nu)$. Thus, the strongest localization of a QB with fixed effective nonlinear parameter ν should be obtained for wave numbers $k_0 \approx \pi/2$. The increase of the effective nonlinearity parameter $\nu \sim |\mu|b$ leads to a weaker localization of QBs in k -space, since the absolute value of the slope S decreases. Note that there is a special point for odd N : $k_0 = \pi/2$, $q_0 = (N+1)/2$. For this seed mode, the QB is compact in k -space⁴. Note that a similar mode with $q_0 = (N+1)/2$ was studied for FPU chains in [21].

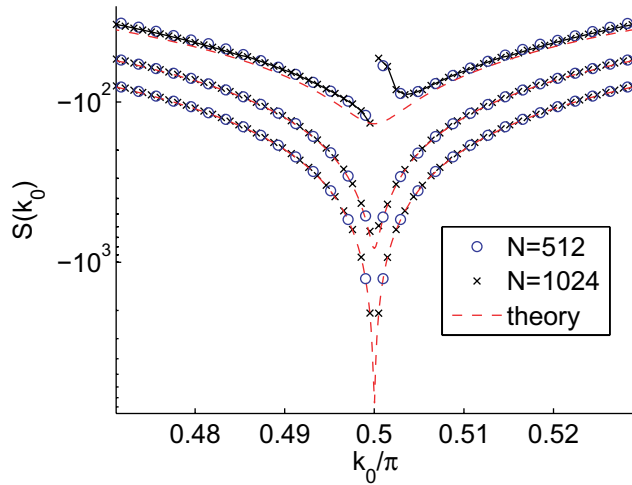


Figure 5. The slope S as a function of the seed wave number k_0 for $d = 1$ with fixed norm density $b = 1/1025$ and $\mu = 0.5, 5$ and 30 (from bottom to top). Dashed lines correspond to the analytical estimates. Different symbols correspond to the estimates of the slopes from numerical calculations of QBs.

In figure 5, the theoretical and numerically obtained dependencies $S(k_0)$ for different values of μ and different system sizes N are plotted. For small values of μ we observe good agreement between analytical and numerical results. But the increase of the nonlinearity leads to a deviation between the theoretical and numerical curves in the region of k_0 close to $\pi/2$. These corrections, as it was for the case of QBs localized near the band edges, depend on the location of k_0 ($k_0 > \pi/2$ or $k_0 < \pi/2$) and on the sign of nonlinearity. Therefore, the curves of $S(k_0)$ for strong nonlinearity ($\mu = 30$) in figure 5 are non-symmetric around the point $k_0 = \pi/2$: in contrast to $k_0 < \pi/2$, for $k_0 > \pi/2$ a local minimum of S is observed. Still, the predicted scaling properties of QBs remain correct even for strong nonlinearity: the values of S , computed for different system sizes N , lie on the same curves for fixed μ .

5.3. Stability of QBs

We analyze the linear stability of QBs as stationary solutions of DNLS model considering the evolution of small perturbations ε_n in the rotating frame of the periodic solution [22]: $\psi_n(t) = (\phi_n^0 + \varepsilon_n(t))\exp(i\Omega t)$, where ϕ_n^0 are the non-perturbed time-independent amplitudes, $\varepsilon_n = \alpha_n + i\beta_n$. A periodic orbit is stable when all perturbations do not grow in time. Solving the linearized equations for the perturbation, that condition translates into the request that all eigenvalues s_m ($m = 1, 2N^d$) of the linearized equations must be purely imaginary. Otherwise the orbit is unstable. In figure 6, we plot the numerical outcome of the stability analysis. We smoothly continue QB solutions for each seed mode number q_0 by increasing the nonlinearity parameter μ and check the stability. If the maximum absolute value of the real parts of all eigenvalues is smaller than 10^{-6} , the QB is considered as stable (solid line), otherwise it is unstable (dashed line), crosses mark the change of stability. For small values of nonlinearity all QBs are stable. Qualitatively different threshold values and dependencies on q_0 for QBs with seed modes from different parts of the spectrum $q_0 < N/2$ and $q_0 > N/2$ are observed. This is

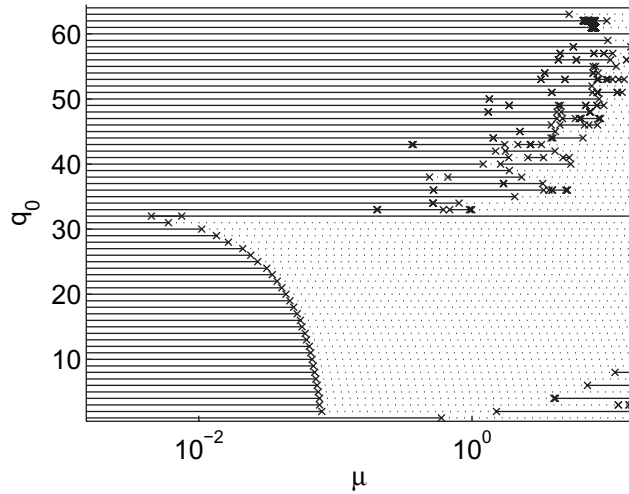


Figure 6. Domain of stability of QBs for $d = 1$. Solid lines, stable; dashed, unstable; crosses, switch from stable to unstable or vice versa. $N = 64$ and $B = 2$.

in agreement with the results presented in [15], where stability properties of nonlinear standing waves are studied. Note that due to the symmetry of the equations, the stability properties of a QB with seed mode q_0 for some negative value of the nonlinearity parameter μ is the same as the stability property of the QB with seed mode $\tilde{q}_0 = N + 1 - q_0$ for the nonlinearity parameter $\tilde{\mu} = -\mu$.

Let us discuss the possible link between linear stability and localization. If a QB becomes delocalized, that happens because of resonances between different mode frequencies. Therefore, we can expect that the same resonances will also drive the state unstable. Indeed, these correlations can be clearly observed from the numerical data. However, if a QB is well localized, it does not follow that it will be stable as well, since instability can arise due to resonant interaction of modes in the breather core alone.

6. Periodic boundary conditions

In the case of periodic boundary conditions, we have used the following transformations between real space and the reciprocal space of normal modes (for even N):

$$\psi_n(t) = \frac{1}{N^{d/2}} \sum_{q_1, \dots, q_d = -N/2+1}^{N/2} Q_q(t) \prod_{l=1}^d \exp\left(i \frac{2\pi q_l (n_l - 1)}{N}\right). \quad (24)$$

The DNLS model (1) with periodic boundary conditions has exact solutions for nonlinear traveling waves, which can be written, for instance in case $d = 1$, as: $\psi_n(t) = \phi_0 \exp(i\Omega t - ik_0 n)$, where $\Omega = -2\cos k_0 - \mu\phi_0^2$, $k_0 = 2\pi q_0/N$ and $q_0 \in [-N/2, N/2]$. These types of solutions can be considered as compact QBs which contain only one mode q_0 . Traveling modes are also not invariant under time reversal. The continuation of a linear standing wave, consisting of two traveling waves with the same norms and wave numbers: k_0 and $-k_0$, into the nonlinear regime leads to a time-reversible QB solution (see figure 7), which is not compact, and its localization properties are similar to the properties of QBs in the case of fixed boundary

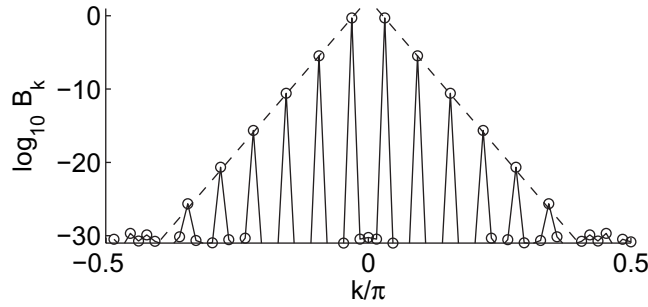


Figure 7. Time-reversible QB in the one-dimensional DNLS model with periodic boundary conditions, continued from the linear standing wave consisting of two traveling waves with $q_0 = 2$ and $q_0 = -2$, $N = 64$, $B = 1$ and $\mu = 0.1$. Dashed lines represent analytical estimations.

conditions. Here, we present the result for decay of mode norms $\lambda_d^{(i)}$ for the case $|k_{i,0}| \ll \pi$, which differs from (10) by a prefactor:

$$\sqrt{(\lambda_d^{(i)})} = \frac{|\mu| A_{q_0}^2 N^{2-d}}{32\pi^2 (q_{i,0})^2} = \frac{|\mu| b_{k_0}}{8(k_{i,0})^2}, \quad i = \overline{1, d}, \quad (25)$$

where $b_{k_0} = B_{k_0}/N^d$ and $k_{i,0} = 2\pi q_{i,0}/N$. Figure 7 illustrates good quantitative agreement between analytical and numerical results obtained for small enough values of norm and nonlinearity.

7. QBs in two- and three-dimensional lattices

For two- and three-dimensional symmetric DNLS lattices (1) with fixed boundary conditions, only linear modes with mode numbers \mathbf{q} on the main diagonal have non-degenerate frequencies. Using the implicit function theorem [19], it follows that these modes are continued into the nonlinear regime. However, we also successfully performed numerical continuations of QBs with seed mode numbers off the main diagonal as was done in [12] for the FPU model. For the two-dimensional DNLS model the QB, continued from the single linear mode $\mathbf{q}_0 = (2, 3)$, is presented in figure 8 in real space (a) and in q -space (b). The QB with the seed mode $\mathbf{q}_0 = (3, 2)$ exists as well and has the same frequency. The slowest decay of the mode norms happens to be along the direction of the main axes. The decay is exponential and in good agreement with the analytical estimation (10) for $d = 2$. In addition to such asymmetric single mode QBs it is possible to construct multi-mode QBs continued from a pair of degenerate linear normal modes (q_0, p_0) and (p_0, q_0) ($q_0 \neq p_0$) with the same norms in both modes and in-phase (figure 8(c)) or antiphase (figure 8(d)) oscillations. It is important to note that the problem of degenerate frequencies is avoided for these solutions. Indeed, system (4) has two invariant manifolds $Q_{q_1, q_2} = \pm Q_{q_2, q_1}$. Looking for a solution on a manifold, the number of independent variables of state is reduced from N^2 to the dimensionality of the manifold, which equals $(N^2 + N)/2$ for the symmetric manifold and $(N^2 - N)/2$ for the antisymmetric one. The reduced system of equations contains only modes with non-degenerate frequencies.

For $d = 3$, we have also verified that the analytical estimations of mode norm decay (10), (14) agree well with the results of numerical calculations for single-mode QBs.

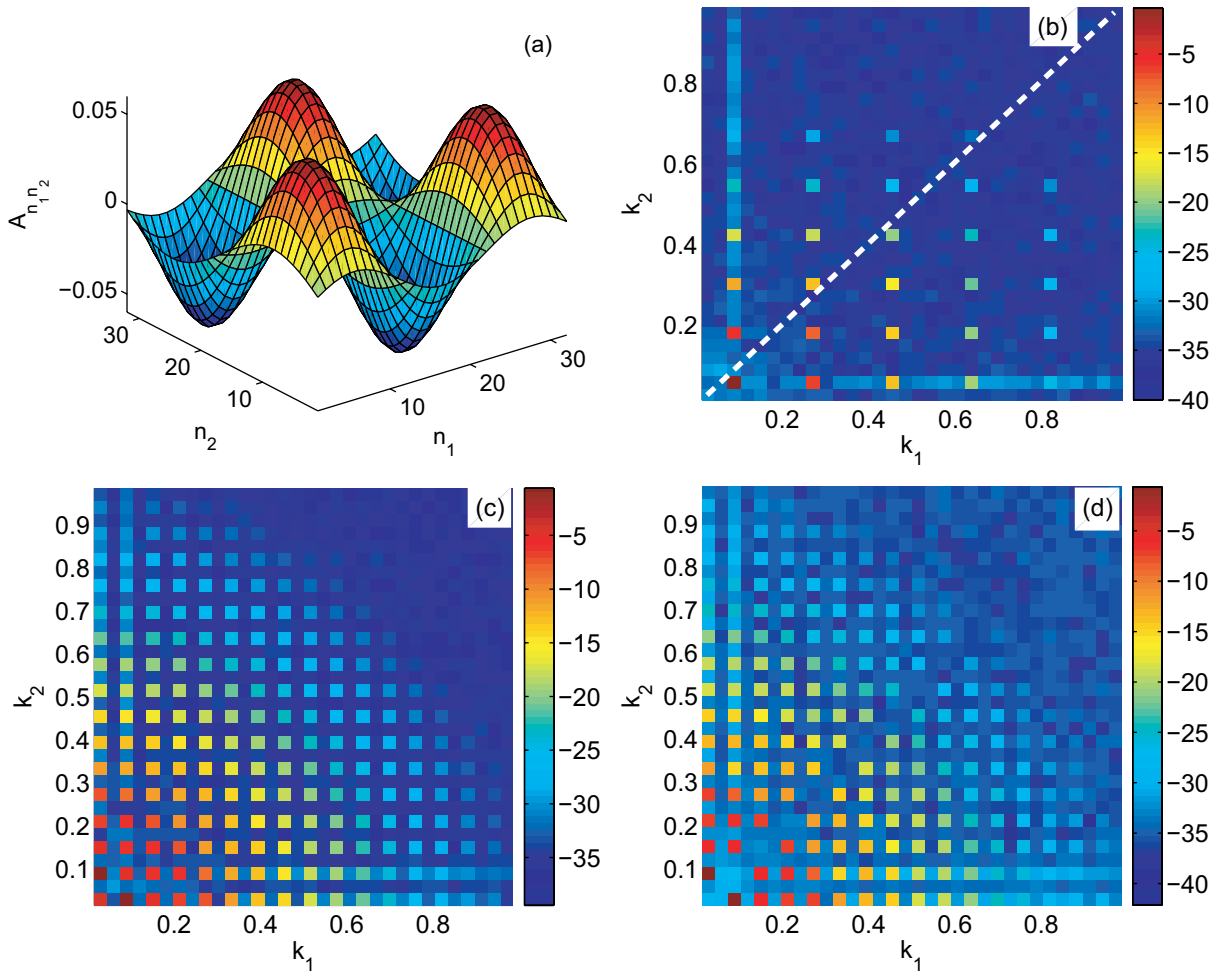


Figure 8. Different QB modes for $d = 2$: $N = 32$, $B = 1$ and $\mu = 0.5$. Mode norm magnitude is plotted in color code on logarithmic scale (except for (a), where a linear scale is used). (a) and (b) asymmetric single-mode QB with seed mode ($\mathbf{q}_0 = (3, 2)$) in real space (a) and in q -space (b); (c) and (d) symmetric multi-mode QB with in-phase (c) and antiphase (d) seed mode pair $\mathbf{q} = (3, 1), (1, 3)$. Dashed line in (b) guides the eye along the main diagonal.

In addition to various time-reversible QB solutions, which are constructed in the same way as for $d = 2$, the three-dimensional DNLS model allows also for non-time-reversible ('vortex') multi-mode solutions. Let us consider QB solutions on an invariant manifold of the system (4): $Q_{q_1, q_2, q_3} = \exp(2\pi i/3) Q_{q_3, q_1, q_2} = \exp(4\pi i/3) Q_{q_2, q_3, q_1}$ (note that this manifold has a counterpart with the opposite sign of the phase shifts). On the manifold the number of variables of state is reduced to $(N^3 - N)/3$. We have constructed numerically a vortex QB solution continued from a degenerate triplet of seed modes which have the same norm and a relative phase shift $2\pi/3$: $Q_{q_0, q_0, p_0} = \exp(2\pi i/3) Q_{p_0, q_0, q_0} = \exp(4\pi i/3) Q_{q_0, p_0, q_0}$, $q_0 \neq p_0$. The frequency of such a triplet becomes non-degenerate in the reduced system on the manifold. The energy flows in a vortex-like manner in q -space for such excitations (figure 9).

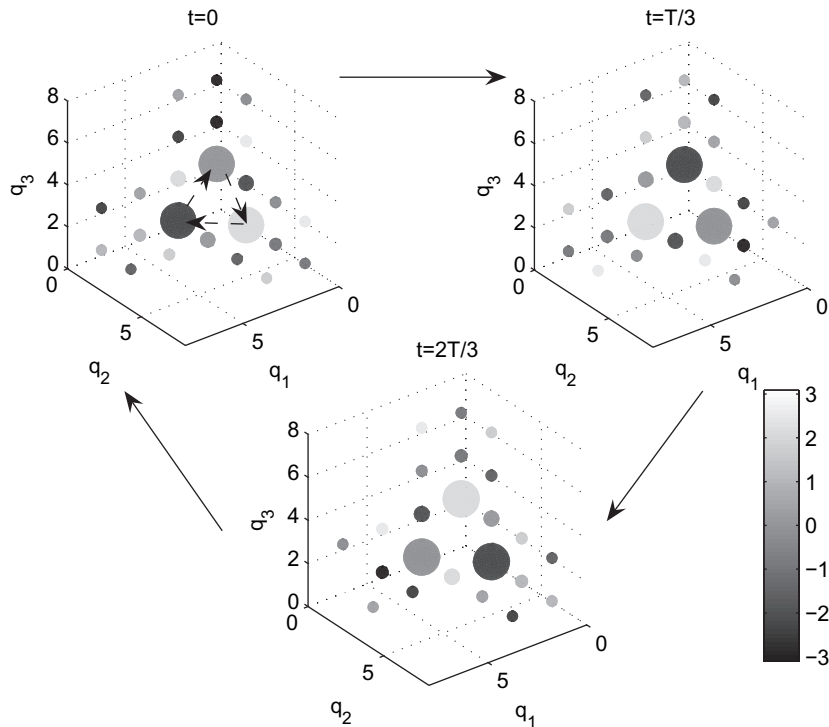


Figure 9. A vortex QB state for $d = 3$: $N = 8$, $B = 1$ and $\mu = 0.1$, at some fixed time. Mode norm magnitude is encoded in sphere sizes on logarithmic scale, while the sphere color denotes the phase of the mode. Seed mode triplet: $\mathbf{q} = (3, 1, 1)$, $(1, 3, 1)$ and $(1, 1, 3)$.

8. QBs and time-periodic multibreather standing waves

The coding of a QB is simple—we need to specify the seed mode number at the limit of zero nonlinearity. Note that the system size is always finite (although it can be chosen to be arbitrarily large). In [15], another approach was taken. There, infinitely large chains were chosen, and standing waves were constructed first in the limit of zero intersite coupling (first term on the rhs in equation (1)). This limit is equivalent to the limit of infinitely strong nonlinearity in our case of fixed intersite coupling strength. The coding of standing waves in that limit is done in real space, by specifying the particular oscillatory state at each lattice site.

In order to study the connection between multibreather states and QBs, we plot in figure 10 (left panel) the continuation of a QB with $q_0 = 1$ when increasing the nonlinearity. We clearly observe that this state transforms smoothly into a single breather localized in real space, while completely delocalizing in q -space. In the right panel we show the outcome of the continuation of a QB with $q_0 = 2$, both for positive and negative nonlinearity. We find that the positive nonlinearity continuation leads to a multibreather with two sites being strongly excited in real space. For negative nonlinearity, the profile flattens in real space, and the continuation ends with a meander-type multibreather where all sites (except one node in the center) are strongly excited. Both results are in full accordance with the predictions of [15].

The above results on the delocalization of QBs close to the band edge happen due to resonances. The multibreather limit yields a simple qualitative interpretation of this delocalization in the one-dimensional case.

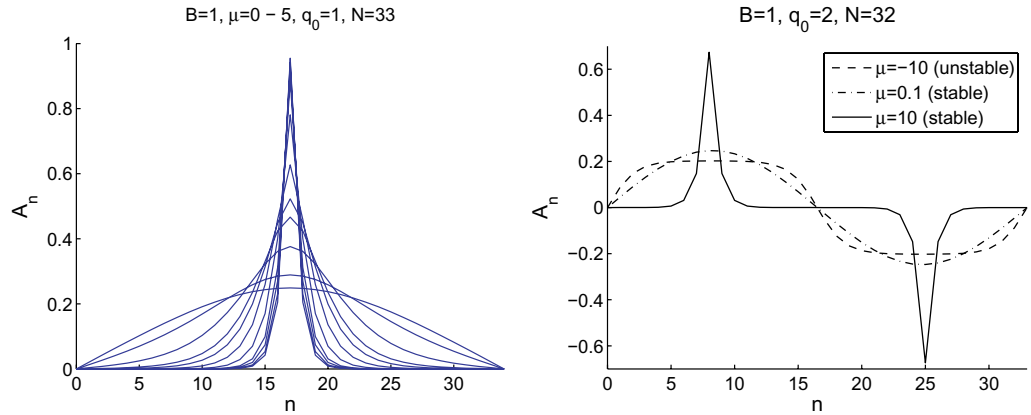


Figure 10. Left panel: continuation of QB with $q_0 = 1$ for $N = 33$, $B = 1$, from $\mu = 0$ to $\mu = 5$. Right panel: same as in left panel, but $q_0 = 2$ and $\mu = -10, 0.1$ and 10.

In two- and three-dimensional lattices we did not find any QB solutions continuable to the multibreather limit. We expect that QBs and multibreathers form different classes of solutions which cannot be continued smoothly into each other, when $d > 1$. However, the detailed description of both classes of solutions when they are continued (frequency–energy dependencies, bifurcations etc) requires separate systematic research.

9. Discussion

Comparing the aims we formulated in the introduction with the above results, we can conclude that indeed the QB concept turns out to be generic, and time-periodic orbits, which are localized in normal mode space, are probably as generic as discrete breathers (although perhaps in a different way). Along with the study of the details of QB properties in DNLS models, we found some particularities, which have not (yet) been obtained in acoustic (FPU) systems. Let us discuss some of these and other findings from above.

9.1. Scales, delocalization thresholds and healing length of a BEC

Let us consider a finite DNLS chain with N sites. Let us fix the total norm density b and the nonlinearity μ . Therefore, we fix the effective nonlinearity parameter $\nu^2 = |\mu|b/16$ (18). If the system size was large enough, we will resolve the extremum in S , and therefore the QB with seed wave number $k_{\min} \approx 2.577\nu$ is the strongest localized one. It evidently sets an inverse length scale ν . This length scale is known in the Gross–Pitaevsky (GP) equation for a BEC in a trap with (similar) fixed boundary conditions. One has a condensate, whose amplitude vanishes at some boundary, yet gets back to some mean value away from the boundary—exactly at the healing length $\xi_h = (4\pi an)^{-1/2}$, where n is the condensate density, and a is the scattering length which is proportional to the atom–atom interaction, and therefore to the nonlinearity strength μ within the mean field GP equation [17]. Therefore, the inverse healing length corresponds to the wave number scale on which the most strongly localized QB is observed.

We now increase the system size further, and compute the localization length (or respectively its negative inverse—the slope S) of the longest wavelength mode. With increasing N the grid of allowed k -values becomes denser, and at some critical $N_c(\nu)$ the localization

length will reach the finite size of the normal mode space, and the QB delocalizes. With a little algebra it follows that

$$N_c \approx \frac{\pi^2}{2\nu^2}, \quad k_0^{(c)} \approx \frac{2\nu^2}{\pi}. \quad (26)$$

For even larger (and finally infinitely large) lattices the critical value $k_0^{(c)}$ marks a border in k -space: at the given norm density ν , all QBs with seed wave numbers $k \gg k_0^{(c)}$ are localized, while we obtain delocalization for $k \leq k_0^{(c)}$. So there is a layer of delocalized QBs at the band edge, whose width grows according to (26) with growing ν . Modes launched inside this layer (with the given norm density) will quickly spread their energy among many other modes—they will quickly relax. Modes launched outside this layer will stay localized in normal mode space, at least for a sufficiently long time. $k_0^{(c)}$ therefore separates a layer of strongly interacting modes from weakly interacting ones. For large enough effective nonlinearity parameter $\nu \sim 1$ the whole wave number space is filled with strongly interacting normal modes, and the normal mode picture breaks down completely. As long as ν is smaller, the value of $k_0^{(c)}$ sets a new length scale $2\pi/k_0^{(c)}$, which is proportional to the *squared* healing length ξ_h^2 . On that new length scale, the normal mode picture breaks down.

9.2. Delocalization thresholds and modulational instability

It is instructive to remember that delocalization thresholds of QBs are related to resonances. Indeed, in the present case, the density of states at the band edge diverges in the limit of large system size, and many modes have almost the same frequencies. It is these small differences, which tend to zero as $1/N^2$, which are responsible for the resonant mode–mode interaction. Notably the analysis of stability of band edge modes [23] (note: for periodic boundary conditions) shows some interesting correlations. The analyzed band edge modes are compact in normal mode space, yet they undergo a tangent bifurcation at amplitudes which are smaller, the larger the system size is. These instabilities appear however only for a certain sign of the nonlinearity, which exactly corresponds to the actual observed delocalization of QBs. Therefore we expect that the (so far not studied) case of a FPU chain with negative quartic nonlinearity, which is known not to yield an instability for the band edge mode, will not show delocalization of QBs close to the (upper) band edge. It is furthermore instructive that if a tangent bifurcation of a band edge mode takes place, the simulation of a lattice shows the onset of modulational instability, which leads to a collection of energies in smaller system volumes, and finally to the formation of discrete breathers—i.e. to localization in real space. Thus we may expect that the resonant layer of strongly interacting modes may lead to the formation of localized states in real space, while the rest of the normal mode space is evolving in the regime of localization in normal mode space. Thus, we may expect to observe in an actual simulation localization *both* in normal mode space *and* in real space.

9.3. Comparing analytical and numerical results

While the delocalization at one band edge, as predicted by perturbation theory, is reproduced by numerical data, that does not happen at the second band edge (both band edges change their places, when the nonlinearity inverts sign). The breakdown of perturbation theory follows from comparing the leading and next-to-leading order terms in the expansion. When terms are of

the same order, we conclude that the series will diverge, and therefore the QB solutions will delocalize. This is true for the case when all terms in the series have the same sign. However, when the terms have alternating sign, the above conclusion must not be correct. And indeed the numerical data show that these sign alternations lead to an effective cancelation, and a final strong localization of a QB solution. We obtained a similar result for QBs in the β -FPU model with a soft interaction potential ($\beta < 0$): the slope function near the lower band edge exhibits no minima, in contrast to the case of hard potential ($\beta > 0$) [13], cf figure 2. A similar breakdown of perturbation theory happens for QB solutions localized at the band center for large nonlinearity (or norm). The perturbation theory tells us that QB states are well localized from both sides of the center. Numerical data, however, show that this is true only on one side from the center, while the other side shows a tendency towards delocalization.

9.4. Open questions

Below we list some potentially interesting and important open questions. Firstly, the influence of different boundary conditions has not been systematically studied. QBs are extended states in real space, therefore their spectrum, and the way they interact, may to some extent be sensitive to the choice of boundary conditions.

A systematic study of multibreather states in two- and three-dimensional systems, and possibilities of their connection to QBs from the present work, could lead to interesting new insights.

Secondly, what kind of excitation we catch by considering a vortex state in normal mode space remains completely open. The existence of vortices of discrete breathers in real space for two-dimensional lattices was observed in [24]. Are our QB vortices related to corresponding states? Clearly the present vortices can be very strongly localized in q -space, but perhaps may also be continued into more delocalized structures, which compactify in real space.

Finally, it would be interesting to see the changes in the QB properties when the norm conservation is lifted. In general, we expect that this will lead to the generation of higher harmonics, and new types of resonances. In fact, it is exactly resonances due to higher harmonics which give the leading order contribution to the FPU problem. However, for sufficiently narrow optical bands, higher harmonics will be located outside the optical band. These resonances will therefore be important when the optical band is wide, or when one considers a complex and broader band structure.

Acknowledgments

Part of this work was completed while SF was visiting the Institute for Mathematical Sciences, National University of Singapore in 2007. KM, OK and MI acknowledge support from RFBR, grants no. 06-02-16499 and 07-02-01404.

References

- [1] Fermi E, Pasta J and Ulam S 1955 *Los Alamos Report LA-1940*
Segre E (ed) 1965 *Collected Papers of Enrico Fermi* vol II (Chicago, IL: University of Chicago Press) pp 977–8
Mattis D C (ed) 1993 *Many-Body Problems* (Singapore: World Scientific)
- [2] Galgani L and Scotti A 1972 *Phys. Rev. Lett.* **28** 1173

- [3] Berchiolla L, Giorgilli A and Paleari S 2004 *Phys. Lett. A* **321** 167
- [4] Izrailev F M and Chirikov B V 1966 *Sov. Phys. Dokl.* **11** 30
- [5] Zabusky N J and Kruskal M D 1965 *Phys. Rev. Lett.* **15** 240
- [6] De Luca J, Lichtenberg A and Lieberman M A 1995 *Chaos* **5** 283
- [7] Ford J 1992 *Phys. Rep.* **213** 271
Campbell D K, Rosenau P and Zaslavsky G M (ed) 2005 Focus issue: The Fermi–Pasta–Ulam problem—The first fifty years *Chaos* **15** 015101
- [8] Sievers A J and Takeno S 1988 *Phys. Rev. Lett.* **61** 970
Dauxois T, Peyrard M and Willis C R 1992 *Physica D* **57** 267
Flach S and Willis C R 1993 *Phys. Lett. A* **181** 232
- [9] Ovchinnikov A A 1970 *Sov. Phys.—JETP* **57** 147
- [10] MacKay R S and Aubry S 1994 *Nonlinearity* **7** 1623
Aubry S 1997 *Physica D* **103** 201
Flach S and Willis C R 1998 *Phys. Rep.* **295** 192
Dauxois T, Litvak-Hinenzon A, MacKay R S and Spanoudaki A (ed) 2004 *Energy Localization and Transfer* (Singapore: World Scientific)
Flach S and Gorbarch A V 2008 *Phys. Rep.* at press
- [11] Flach S, Ivanchenko M V and Kanakov O I 2005 *Phys. Rev. Lett.* **95** 064102
Flach S, Ivanchenko M V and Kanakov O I 2006 *Phys. Rev. E* **73** 036618
Penati T and Flach S 2007 *Chaos* **17** 023102
Flach S and Ponno A 2007 *Physica D* **237** 908
Flach S, Ivanchenko M V, Kanakov O I and Mishagin K G 2008 *Am. J. Phys.* **76** 453
- [12] Ivanchenko M V, Kanakov O I, Mishagin K G and Flach S 2006 *Phys. Rev. Lett.* **97** 025505
- [13] Kanakov O I, Flach S, Ivanchenko M V and Mishagin K G 2007 *Phys. Lett. A* **365** 416
Flach S, Kanakov O I, Mishagin K G and Ivanchenko M V 2007 *Int. J. Mod. Phys. B* **21** 3925
- [14] Kivshar Y S and Peyrard M 1992 *Phys. Rev. A* **46** 3198
Johansson M 2006 *Physica D* **216** 62
- [15] Morgante A A, Johansson M, Kopidakis G and Aubry S 2002 *Physica D* **162** 53
Johansson M, Morgante A M, Aubry S and Kopidakis G 2002 *Eur. Phys. J. B* **29** 279283
- [16] Pitaevskii L P 1961 *Sov. Phys.—JETP* **13** 451
Gross E P 1961 *Nuovo Cimento* **20** 454
- [17] Morsch O and Oberthaler M 2006 *Rev. Mod. Phys.* **78** 179
- [18] Kivshar Yu S and Agrawal G P 2003 *Optical Solitons: From Fibers to Photonic Crystals* (Amsterdam: Elsevier)
- [19] Dieudonne J 1999 *Foundations of Modern Analysis* (New York: Academic)
- [20] Bivins R L, Metropolis N and Pasta J R 1973 *J. Comput. Phys.* **12** 65
Chechin G M, Novikova N V and Abramenko A A 2002 *Physica D* **166** 208
Rink B 2002 *Physica D* **175** 31
- [21] Antonopoulos C and Bountis T 2006 *Phys. Rev. E* **73** 056206
- [22] Gorbach A V and Johansson M 2004 *Eur. Phys. J. D* **29** 77
- [23] Budinsky N and Bountis T 1983 *Physica D* **8** 445
Sandusky K W and Page K B 1994 *Phys. Rev. B* **50** 866
Flach S 1996 *Physica D* **91** 223
Dorignac J and Flach S 2005 *Physica D* **204** 83
- [24] Cretegny T and Aubry S 1997 *Phys. Rev. B* **55** R11929